

AD-A110 197 ROCKWELL INTERNATIONAL THOUSAND OAKS CA ELECTRONICS--ETC F/6 20/3

TEMPERATURE COMPENSATED PIEZOELECTRIC MATERIALS. (U)

JAN 81 R R NEURGAONKAR

F49620-78-C-0093

UNCLASSIFIED

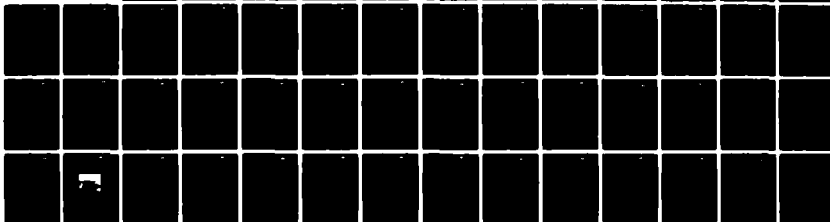
ERC41007.145A

AFOSR-TR-81-0896

NL

1-1

1-1



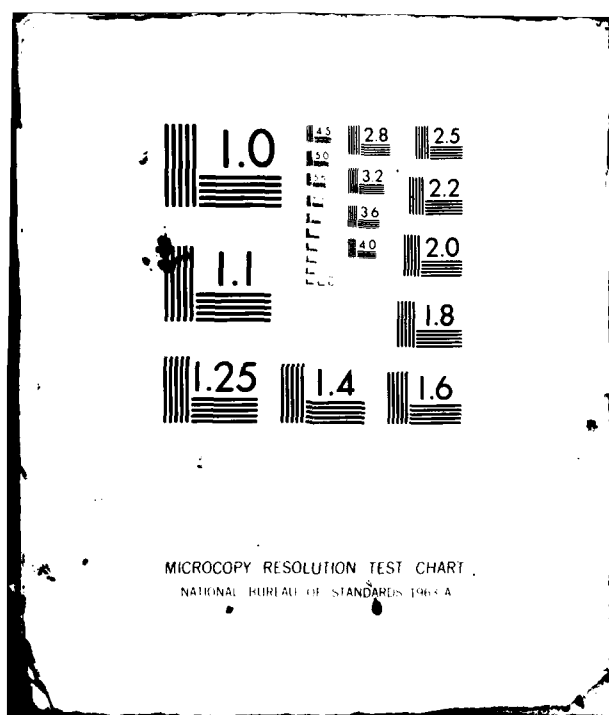
END

DATE

FILED

2 82

DTIC



AD A110197

DTIC FILE COPY

January 1981

ERC41007.14SA

TEMPERATURE COMPENSATED PIEZOELECTRIC MATERIALS

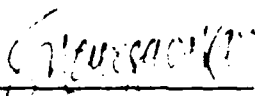
Semi-Annual Technical Report #3
For Period 05/15/80 through 11/30/80

Contract No. F49620-78-C-0093

General Order No. 41007

Prepared for

Air Force Office of Scientific Research
Bolling Air Force Base
Washington, D.C. 20332


R. R. Neurgaonkar
Principal Investigator

82

01



Rockwell International

Approved for release;
distribution unlimited.

UNCLASSIFIED

SECURITY CLASSIFICATION OF THIS PAGE (When Data Entered)

REPORT DOCUMENTATION PAGE		READ INSTRUCTIONS BEFORE COMPLETING FORM
1. REPORT NUMBER AFOSR-TR- 31 - 0896	2. GOVT ACCESSION NO. AD-A110197	3. RECIPIENT'S CATALOG NUMBER
4. TITLE (and Subtitle) TEMPERATURE COMPENSATED PIEZOELECTRIC MATERIALS		5. TYPE OF REPORT & PERIOD COVERED Semi-Annual Technical Report 05/15/80 through 11/30/80
7. AUTHOR(s) R. R. Neurgaonkar		6. PERFORMING ORG. REPORT NUMBER ERC41007.14SA
9. PERFORMING ORGANIZATION NAME AND ADDRESS Rockwell International Microelectronics Research & Development Center 1049 Camino Dos Rios Thousand Oaks, CA 91360		8. CONTRACT OR GRANT NUMBER(s) F49620-78-C-0093
11. CONTROLLING OFFICE NAME AND ADDRESS Air Force Office of Scientific Research Bolling Air Force Base Washington, D.C. 20332		10. PROGRAM ELEMENT, PROJECT, TASK AREA & WORK UNIT NUMBERS 6110LF 35TC/01
14. MONITORING AGENCY NAME & ADDRESS (if different from Controlling Office)		12. REPORT DATE January 1981
		13. NUMBER OF PAGES 53
		15. SECURITY CLASS. (of this report) Unclassified
		15a. DECLASSIFICATION/DOWNGRADING SCHEDULE
16. DISTRIBUTION STATEMENT (of this Report) Approved for public release; distribution unlimited.		
17. DISTRIBUTION STATEMENT (of the abstract entered in Block 20, if different from Report)		
18. SUPPLEMENTARY NOTES		
19. KEY WORDS (Continue on reverse side if necessary and identify by block number) <div style="display: flex; justify-content: space-between;"> <div> Strontium barium niobates Liquid phase epitaxy Czochralski growth technique </div> <div> Gibb's energy functions Phenomenological model Elastic compliances </div> </div>		
20. ABSTRACT (Continue on reverse side if necessary and identify by block number) <p>From the electrostriction measurements on SBN crystals, it was found that the fourth order electrostrictive coupling terms are not adequate to fully describe the paraelectric phase above Curie temperature, and hence six rank coupling terms are needed; the electrostrictive coupling terms do not change markedly with cation substitution. Several flux systems have successfully been developed for the liquid phase epitaxy work of SBN compositions. The work is successful, and it is possible to develop epilayers of SBN compo-</p>		

DD FORM 1 JAN 73 1473

EDITION OF 1 NOV 65 IS OBSOLETE

UNCLASSIFIED

Compositions

SECURITY CLASSIFICATION OF THIS PAGE (When Data Entered)



TABLE OF CONTENTS

	<u>Page</u>
1.0 PROGRESS AND TECHNICAL REPORT SUMMARY.....	1
2.0 THERMODYNAMIC PHENOMENOLOGY.....	3
2.1 Introduction.....	3
2.2 Thermodynamic Phenomenology.....	5
2.3 Procedure for Determining Thermodynamic and Electro-Acoustical Constants.....	12
2.4 Experimental Results and Discussion.....	15
2.5 Conclusion.....	26
3.0 MATERIALS PREPARATION AND CHARACTERIZATION.....	28
3.1 Single Crystal Growth of $\text{Sr}_{.61}\text{Ba}_{.39}\text{Nb}_2\text{O}_6$	28
3.2 Characterization of Bulk Single Crystals.....	29
3.2.1 Poling Procedure.....	29
3.2.2 Method for Evaluating Electromechanical Constants.....	32
3.3 Liquid Phase Epitaxial Growth of $\text{Sr}_{1-x}\text{Nb}_2\text{O}_6$	34
3.4 Crystal Chemistry of PbNb_2O_6	38
4.0 FUTURE PLANS.....	43
4.1 Application of Phenomenological Model.....	43
4.2 Material Preparation and Acoustical Characterization.....	43
4.3 Electro-optic Measurements.....	44
4.4 Crystal Chemistry.....	44
5.0 PUBLICATION AND PRESENTATIONS.....	45
5.1 Publications.....	45
5.2 Presentations.....	46
6.0 REFERENCES.....	48

ATTENTION: CONTRACT ADMINISTRATION (AFSC)

1115

12.

CHRYSLER CORPORATION, Rockwell International Division



LIST OF FIGURES

	<u>Page</u>
Fig. 1 Shapes and orientations of specimen.....	13
Fig. 2 Elastic compliances of S_{11}^E , S_{11}^P and $S_{11}^{E'}$, $S_{11}^{P'}$ as function of induced electrical polarization in SBN measured at 121°C....	16
Fig. 3 Measured values of rotated and unrotated cuts over a range of temperature above T_c	17
Fig. 4 Comparison of the measured P_s in SBN and distribution function values.....	20
Fig. 5 Measured weak field permittivity ϵ_{33} for SBN compared to the calculated using the distributed LGD model.....	21
Fig. 6 Measured and desired thermal expansion α_3	22
Fig. 7 S_{ij}^P measured from piezo-electric response data compared to S_{ij}^P derived using α_{3ij} values determined in the paraelectric phase.....	24
Fig. 8 Idealized form of the SBN single crystals.....	30
Fig. 9 Capacitance as a function of temperature for the SBN single crystal.....	31
Fig. 10 Electromechanical coupling constant as a function of applied field.....	33
Fig. 11 The temperature coefficient of time delay for the z-cut SBN surface wave delay lines.....	35
Fig. 12 Shows a typical cross section of the $Sr_{.5}Ba_{.5}Nb_2O_6$ film on the Z-cut SBN substrate.....	37
Fig. 13 The system BaV_2O_6 - $SrNb_2O_6$ - $BaNb_2O_6$, in air at 1200°C.....	39
Fig. 14 Variation of ferroelectric transition temperature for the $Pb_{1-2x}K_xLa_xNb_2O_6$ system.....	42

iii

Accession For	<input checked="" type="checkbox"/>	<input type="checkbox"/>	<input type="checkbox"/>
DTIC			
DTIC TAB			
Unannounced			
Justification			
Distribution/			
Availability Codes			
Avail and/or			
Spec			
Special			





LIST OF TABLES

<u>Table</u>	<u>Page</u>
1. Determined Thermodynamic Parameters.....	18
2. Physical Constants of SBN at Room Temperature.....	25
3. Electromechanical Coupling Constant K^2 for SBN Crystals.....	34
4. The Solid-solution Based on the $\text{Pb}(\text{Nb}_{2/3}\text{Sb}_{1/3})\text{O}_6$	40



1.0 SUMMARY

The objective of the present research investigations is to establish the physics of why known ferroelectric and ferroelastic materials are temperature-compensated and through this understanding predict such occurrences. Physical knowledge from such findings will be used to grow and characterize suitable phases of the tungsten bronze family. The end goal is to develop high-coupling, temperature-compensated materials for minimum shift keyed surface wave filters.

The Landau:Ginsburg:Devonshire phenomenological theory for proper ferroelectrics has been extended to include sixth order electrostrictive coupling in the prototype structure. These higher order terms lead to contributions to the stiffened elastic compliances, S_{ijkl}^P , which are quadratic in polarization p , so that in the ferroelectric phase strong temperature dependence of p_s , the spontaneous polarization, is reflected onto elastic response. The analysis has been applied to the tungsten bronze ferroelectric $\text{Sr}_{.61}\text{Ba}_{.39}\text{Nb}_2\text{O}_6$ and the sixth order electrostriction constants measured in the prototype phase used to derive elastic behavior in the ferroelectric form. A feature which makes the phenomenology valuable is that the higher order stiffnesses and coupling terms do not change markedly with temperature or with cationic makeup, thus in principle it is possible to predict from a single family of prototypic constants quantitative trends for the dielectric, piezoelectric, elastic and thermal constants for a very wide range of bronze ferroelectric compounds.



ERC41007.14SA

Ferroelectric $\text{Sr}_{.61}\text{Ba}_{.39}\text{Nb}_2\text{O}_6$ single crystals approximately 2.5 cm and 4 cm long have successfully been grown by the Czochralski technique. This technique is well established for this composition and we continue to improve the quality and size of grown crystals. The SAW electromechanical coupling constant, K^2 , for three different cuts, e.g. (100), (110) and (001) of $\text{Sr}_{.61}\text{Ba}_{.39}\text{Nb}_2\text{O}_6$ single crystals has successfully been determined. This coupling constant has been shown to be large for the (001) plane propagating along the $\langle 110 \rangle$ direction; its value is measured to be 422×10^{-4} , which is comparable to the Y-Z cut LiNbO_3 (480×10^{-4}).

The liquid phase epitaxial (LPE) growth technique to develop thin films of $\text{Sr}_{.5}\text{Ba}_{.5}\text{Nb}_2\text{O}_6$ on the Z-cut of SBN substrate has successfully been established. This is the first time such films have been developed for acoustical studies. The work has currently been extended to initiate the LPE growth of this composition on other cuts such as (100), (110), (111), etc.

Electro-optic measurements are also in progress to establish r_{13} and r_{33} coefficients for the $\text{Sr}_{.61}\text{Ba}_{.39}\text{Nb}_2\text{O}_6$ single crystals. Once this is established, the crystals will be tested for electro-optic Fabry-Perot spectral filter applications.

The temperature dependence dielectric measurements on solid solution $\text{Pb}_{1-2x}\text{K}_x\text{La}_x\text{Nb}_2\text{O}_6$ showed that the ferroelectric phase transition temperature, T_c , decreases in both the orthorhombic and tetragonal tungsten bronze phases with increasing concentration of $\text{K}^+ + \text{La}^{3+}$ in PbNb_2O_6 . Further work to establish this system's piezoelectric properties is in progress.



2.0 THERMODYNAMIC PHENOMENOLOGY

2.1 Introduction

For many acoustic wave devices it is desirable that the propagation time τ for the elastic wave be independent of ambient temperature change. The temperature coefficient of delay for a bulk wave may be simply written¹

$$\frac{1}{\tau} \left(\frac{\partial \tau}{\partial T} \right)_X = \alpha_L - \frac{1}{2} \alpha_V - \frac{1}{2} \frac{1}{c} \left(\frac{\partial c}{\partial T} \right)_X \quad (1)$$

where τ is the propagation (or delay) time measured at constant stress X , α_L the coefficient of linear thermal expansion in the direction of propagation, α_V the volume coefficient of expansion, and c a combination of elastic constants depending on the type, polarization, and propagation direction of the elastic wave.

It is evident from Eq. (1) that for a material to be temperature compensated it should possess either a positive temperature coefficient of an elastic constant or a negative coefficient of thermal expansion. Quartz, berlinite and β -eucryptite are examples of known temperature compensated piezoelectric materials which do have at least one positive temperature coefficient of an elastic constant or in the case of β -eucryptite a negative thermal expansion.

In the design of broad bandwidth device structures not only temperature compensated materials are required, but piezoelectric materials with larger piezoelectric coupling (k_{ij}) than quartz and low impedance (high permittivity (ϵ_{ij})) are desired. In the search for such materials it is natural to explore the tungsten bronze family of ferroelectrics in which one



finds suitable magnitudes of k and ϵ and the possibility of temperature compensation as evidenced by negative thermal expansion coefficients. In the tetragonal bronze family one also finds over 100 known individual ferroelectric compounds and innumerable² possible solid solutions between these end members. The paraelectric prototype point symmetry is $4/mmm$ with only 2 different ferroelectric forms known: an orthorhombic form in which the spontaneous polarization (P_s) is along 110 , $1\bar{1}0$, $\bar{1}10$, or $1\bar{1}\bar{0}$, which is in polar point group $mm2$ symmetry and a tetragonal form in which P_s lies along 001 or $00\bar{1}$ and which has polar tetragonal $4mm$ symmetry.

To characterize the elastic wave behavior completely in the orthorhombic or tetragonal case involves measuring many elastic, piezoelectric, and dielectric constants and their temperature derivatives and including thermal expansion coefficients.

Clearly, if this measurement burden were to be repeated for each member compound of interest and iterated across each solid solution the task of choosing an optimum bronze for elastic wave application would be horrendous. In earlier work Cross et al³ proposed a more rational guideline by making use of Landau:Ginsburg:Devonshire (LGD) thermodynamic phenomenology for simple proper* ferroelectrics. By extending the LGD phenomenology to

*Proper as distinct from improper or extrinsic ferroelectrics are characterized by the fact that the electric spontaneous polarization (P_s) is an effective order parameter describing the phase change from paraelectric to ferroelectric form. Changes or properties in the ferroelectric phase can be traced to essential consequences of onset of polarization in the paraelectric phase and their temperature dependence can be described by a simpler family of temperature independent coupling parameters in the paraelectric prototype.



include sixth order elasto-electric coupling terms it was found for the ferroelectric tungsten bronze ($\text{Sr}_{0.61}\text{Ba}_{0.39}\text{Nb}_2\text{O}_6$) that the stiffened elastic constants S_{ij}^P were strongly influenced by the electric polarization and their temperature dependence could be predicted from the measured sixth order para-electric constants.

The phenomenology is potentially valuable in that the higher order dielectric stiffnesses and coupling terms do not change markedly with temperature or with cationic makeup, making it possible in principle to predict semiquantitatively the trends for the dielectric, thermal, piezoelectric, and elastic constants for a wide compositional range of ferroelectric bronze compounds from a very limited set of prototypic constants.

In the preliminary work by Cross et al only a partial set of higher order coupling terms and other thermodynamic constants were reported. It is the purpose of this paper to show again the importance of the sixth order coupling terms for the elastic behavior of simple proper ferroelectrics and to present a more complete set of thermodynamic and electro-acoustical parameters for $\text{Sr}_{0.61}\text{Ba}_{0.39}\text{Nb}_2\text{O}_6$. A simplified review of the LGD phenomenology is also presented. Detailed descriptions of the phenomenology are reported elsewhere.⁴

2.2 Thermodynamic Phenomenology

In general, the thermodynamic function of interest to describe the isothermal, isobaric properties of a polarizable deformable insulator is the elastic Gibbs function G_1 defined by



ERC41007.14SA

$$G_1 = U - TS - Xx \quad (2)$$

where U is the internal energy, S the entropy, T the temperature, X the elastic stress, and x the strain. The increment of G_1 , dG_1 will be made up from

$$dG_1 = -SdT - xdX + EdP \quad (3)$$

where E is the electric field, P the electric polarization and E and P are polar vectors. Thus from the partial derivatives of G_1 we may derive the strain x , elastic compliance at constant P (s^P), electric field (E), dielectric stiffness (X^X), piezoelectric polarization constant (b) etc.

It is conventional in Landau:Ginsburg:Devonshire phenomenological theory to take out the elastic Gibbs energy of the unpolarized undeformed crystal and write

$$\Delta G_1 = G_1(\text{polarized}) - G_1(\text{unpolarized}) = f(P, X, T) \quad (4)$$

and to separate the function f into three components

$$\Delta G_1 = f(P, T) + f(X, T) + f(X, P) \quad (5)$$

Inserting now the vector nature of P and E , and the tensor form of Xx , $f(P, T)$ is expressed as a power series expansion



$$f(PT) = \alpha_{ij} P_i P_j + \alpha_{ijk} P_k P_j P_k + \dots \quad (6)$$

where the α_{ijk} are limited by the prototype symmetry and only the $\alpha_{ij,s}$ are temperature dependent. If the ferroelectric transition is first order, it is necessary to include at least the first 6th power terms in P.

Usually only "Hookian" elastic behavior is considered and $f(XT)$ takes the simple form

$$f(X,T) = -\frac{1}{2} s_{ijkl} X_{ij} X_{kl} \quad (7)$$

It has been considered necessary only to include the lowest power symmetry allowed coupling terms between P and X, so that $f(XP)$ is given by either

$$f(X,P) = -b_{ijk} P_i X_{jk} \quad (8)$$

or

$$f(X,P) = -Q_{ijkl} P_i P_j X_{kl} \quad (9)$$

where Q_{ijkl} are the symmetry permitted electrostriction constants.

For centric prototype structures of the type to be considered all $b_{ijk} \equiv 0$, and the phase change at T_c is first order. Since 6th power terms in P are absolutely necessary it seems illogical to consider only the 4th rank coupling terms, and we propose to add terms of the form



ERC41007.14SA

$$-[\Phi_{ijklmn}P_iP_jX_kX_{mn}] - [W_{ijklmn}P_iP_jP_kP_lX_{mn}] \quad (10)$$

For the elastic behavior clearly the Φ terms are most important. In the unmodified LGD theory in the spontaneously polarized phase taking second partial derivatives with respect to the X_{ij} obviously all Q terms drop out so that

$$s_{klmn}^P(\text{polarized}) = s_{klmn}^P(\text{unpolarized})$$

whereas if the Φ constants have significant magnitude

$$s_{klmn}^P(\text{polarized}) = s_{klmn}^P(\text{unpolarized}) + \Phi_{ijklmn}P_iP_j$$

Since the polarization components P_iP_j in the simple ferroelectric have strong temperature dependence, the electrostrictive term may be most important in dictating temperature dependence for the elastic compliances in the ferroelectric phase.

For the prototype 4/mmm centric group the unmodified LGD elastic Gibbs function has the form [Note: the use of shorter matrix notation (Nye⁵)].



$$\begin{aligned}
\Delta G = & \alpha_1 (P_1^2 + P_2^2) + \alpha_3 P_3^2 + \alpha_{11} (P_1^4 + P_2^4) + \alpha_{33} P_3^4 \\
& + \alpha_{13} (P_1^2 P_3^2 + P_3^2) + \alpha_{12} P_1^2 P_2^2 + \alpha_{333} P_3^6 \\
& + \alpha_{111} (P_1^6 + P_2^6) - \frac{1}{2} S_{11} (X_1^2 + X_2^2) - S_{12} X_1 X_2 \\
& - S_{13} (X_1 + X_2) X_3 - \frac{1}{2} S_{33} X_3^2 - \frac{1}{2} S_{44} (X_4 X_5^2) \\
& - \frac{1}{2} S_{66} X_6^2 - Q_{11} (P_1^2 X_1 + P_2^2 X_2) - Q_{12} (P_1^2 X_2 + P_2^2 X_1) - Q_{13} (P_1^2 X_3 + P_2^2 X_3) \\
& - Q_{31} (P_3^2 X_1 + P_3^2 X_2) \\
& - Q_{33} P_3^2 X_3 - Q_{44} (P_2 P_3 X_4 + P_1 P_3 X_5) \\
& - Q_{66} P_1 P_2 X_6
\end{aligned} \tag{11}$$

From dielectric data in the paraelectric phase α_3 is a linearly decreasing function of temperature passing through zero near the paraelectric-ferroelectric transition (T_c), that is

$$\alpha_3 = \alpha_{30} (T - \theta_3) \tag{12}$$

where θ_3 is close to T_c whereas α_1 also has the same form



$$\alpha_1 = \alpha_{10}(T - \theta_1) \quad (13)$$

but α_1 is very much below T_c .

For the tetragonal ferroelectric (4mm) case when the crystal spontaneously polarizes along the tetrad axis [001] the non-zero isothermal dielectric stiffnesses are (at $X=0$)

$$\chi_{11}^T = \chi_{22}^T = 2\alpha_1 + 2\alpha_{13}P_3^2 \quad (14)$$

$$\chi_{33}^T = 2\alpha_3 + 12\alpha_{33}P_3^2 + 30\alpha_{333}P_3^4$$

The tetragonal spontaneous strains are given by

$$x_1 = x_2 = Q_{31}P_3^2 \quad (15)$$

$$x_3 = Q_{33}P_3^2$$

and the piezoelectric b coefficients by

$$b_{15} = b_{24} = Q_{44}P_3$$

$$b_{31} = b_{32} = 2Q_{31}P_3 \quad (16)$$

$$b_{33} = 2Q_{33}P_3$$



with all other x and b terms equal to zero. The piezo b constants are related to the more frequently used d constant by $d = b/X$.

If the sixth order ϕ terms are added to Eq. (11), then the second derivatives with respect to the stress give the stiffened elastic compliances s_{ij}^P which take the form

$$s_{11}^P(P) = s_{22}^P(P) = s_{11}^P(0) + \phi_{311}P_3^2$$

$$s_{12}^P(P) = s_{12}^P(0) + \phi_{312}P_3^2$$

$$s_{13}^P(P) = s_{23}^P(P) = s_{13}^P(0) + \phi_{313}P_3^2$$

(17)

$$s_{33}^P(P) = s_{33}^P(0) + \phi_{333}P_3^2$$

$$s_{44}^P(P) = s_{55}^P(P) = s_{44}^P(0) + \phi_{334}P_3^2$$

$$s_{66}^P(P) = s_{66}^P(0) + \phi_{366}P_3^2$$

where the suffix (P) indicates the S value at polarization level P and the suffix (0) the prototypic value when $P=0$.



2.3 Procedures for Determining Thermodynamic and Electro-Acoustical Constants

Single crystals of composition $(\text{Sr}_{0.61}\text{Ba}_{0.39})\text{Nb}_2\text{O}_6$ used in this investigation were grown by Czochralski technique. The crystal SBN is a ferroelectric tungsten bronze with T_c at $\approx 72^\circ\text{C}$ and belongs to point group 4mm; above T_c the paraelectric prototype symmetry is 4/mmm.

Due to the large number of parameters needed to fully characterize the system, which includes 6 elastic, 3 piezoelectric, and 2 dielectric constants, several specimens with various shapes and orientations were used (Fig. 1). Prior to measurements, the crystals were poled by the field-cooling method under a DC field of 10 KV/cm along the 001 or z axis.

The procedures for determining elastic and piezoelectric constants were similar to those described by Berlincourt and Jaffe⁶ in the case of BaTiO_3 utilizing the resonance-antiresonance transmission method.⁷

The dielectric constants were measured on the 001 and 100 square plates at 100 KHz using a Hewlett Packard (Model 4270A) automatic capacitance bridge.

The thermal expansion coefficients (α_1 and α_3) were determined using high temperature x-ray diffraction measurements.

The spontaneous polarization (P_s) as a function of temperature was determined statically. An electrically poled sample being equilibrated at some temperature $T(T < T_c)$ was thermally depoled by quenching in a 200°C silicone oil bath while charge was collected using an electrometer.

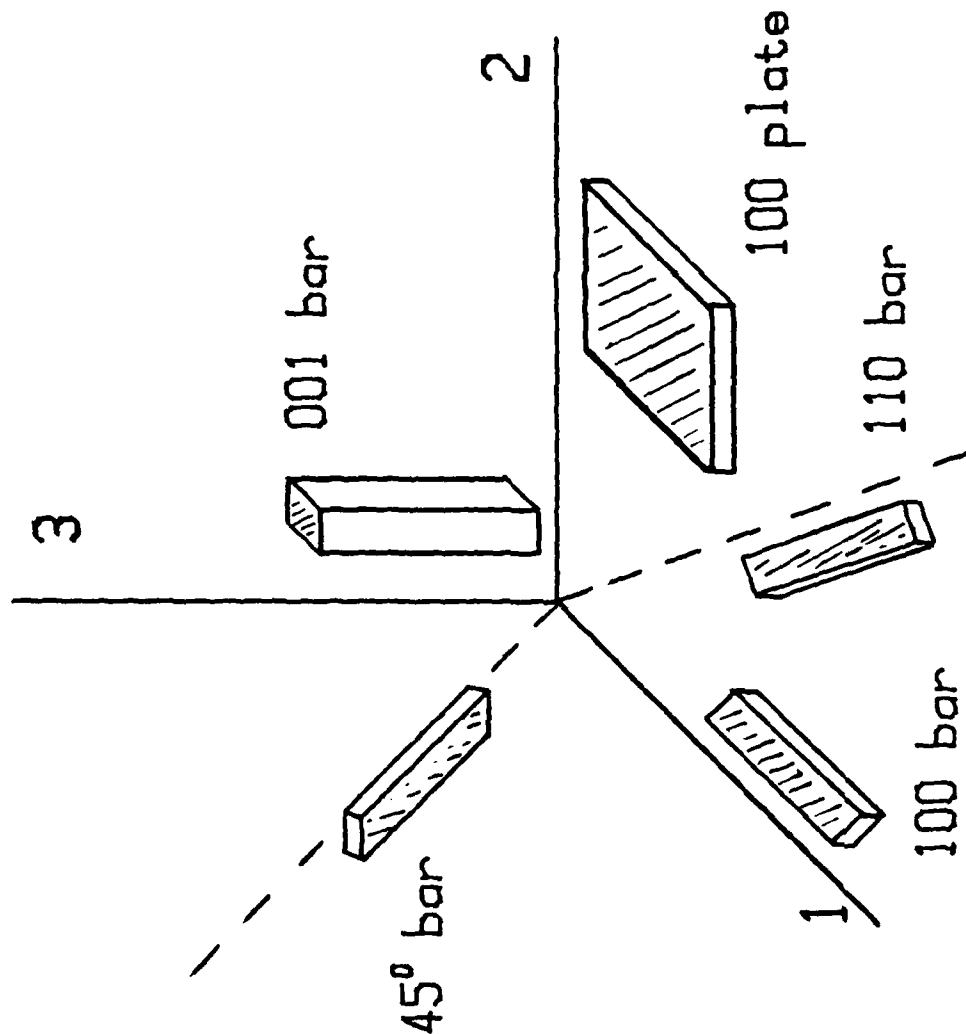


Fig. 1 Shapes and orientations of specimen.



ERC41007.14SA

The higher order ϕ_{3ij} constants were also determined utilizing the resonance-antiresonance method. For temperatures above T_c where $P_s = 0$, an induced piezoelectric resonance was achieved by the application of a DC field.

For a longitudinally vibrating bar, as for the 100, 110, 45° and 30° bars, and the breathing mode of the 100 plate, the elastic behavior is basically related to the appropriate elastic constant, density and the governing dimension as indicated in equation (18).

$$f_R = \frac{1}{2L} \sqrt{\frac{1}{S_{11}^E \rho}} \quad (18)$$

where f_R is the resonant frequency (Note: the prime represents a rotated value). In the case of the 001 bar and thickness mode vibration of the 100 plate the elastic constant (at constant P) is determined from the antiresonance frequency. By repeating the resonant and antiresonant measurements at a sequence of different field levels, different values of P may be induced and a change in the elastic compliance is indicated by a change in the resonant or antiresonant frequency which can be easily and accurately measured. The elastic constants at constant polarization (S^P) and constant field (S^E) are related by the appropriate piezoelectric coupling coefficient through the relationship⁷

$$S^P = S^E (1 - k^2) \quad (19)$$



2.4 Experimental Results and Discussions

Typical measurements of S_{11}^E and S_{11}^P as a function of induced P_3 taken from resonance data on the 100 bar at 121°C are shown in Fig. 2, and of $S_{11}^{'E}$ and $S_{11}^{'P}$ taken from the resonance of the 45° bar (Fig. 2). Clearly, both S_{11}^P and S_{11}^E are linear functions of P^2 and the magnitudes of ϕ_{311} and ϕ_{311}' can be deduced from measurement of the slopes of the S_{11}^P lines.

By repeating measurements of the field (polarization) dependence of the resonances and antiresonances at a sequence of temperatures above T_c , it has been shown that the ϕ_{3ij} (Fig. 3) constants change little with temperature. Thus the importance of the sixth order electrostriction coupling upon the elastic constant in the bronze ferroelectrics is clearly established. The ϕ_{3ij} constants determined from measurements under induced polarization P_3 are listed in Table 1.

Before the LGD phenomenology can be used to correlate the dielectric, piezoelectric, and elastic behavior between the paraelectric and ferroelectric phases a special feature of ferroelectricity in the SBN bronze must be recognized. In the SBN bronze as in many ferroelectric materials, it has been determined⁸ that the phase change at T_c is not abrupt but is diffuse. Thus over limited range of temperature close to T_c paraelectric and ferroelectric phases coexist. The thermodynamic description which has been given above is appropriate for a completely homogeneous crystal which has an abrupt phase

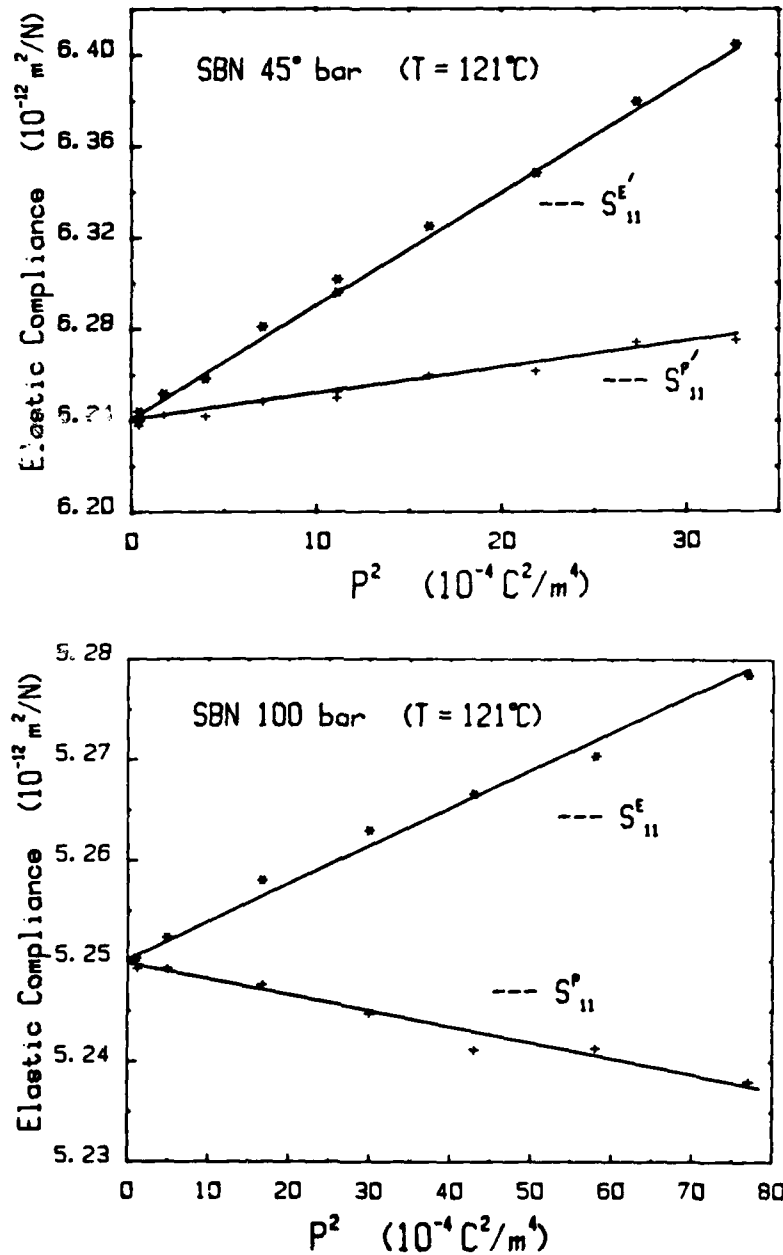


Fig. 2 Elastic compliances of S^E_{11} , S^P_{11} and $S^{E'}_{11}$, $S^{P'}_{11}$ as function of induced electrical polarization in SBN measured at 121°C .

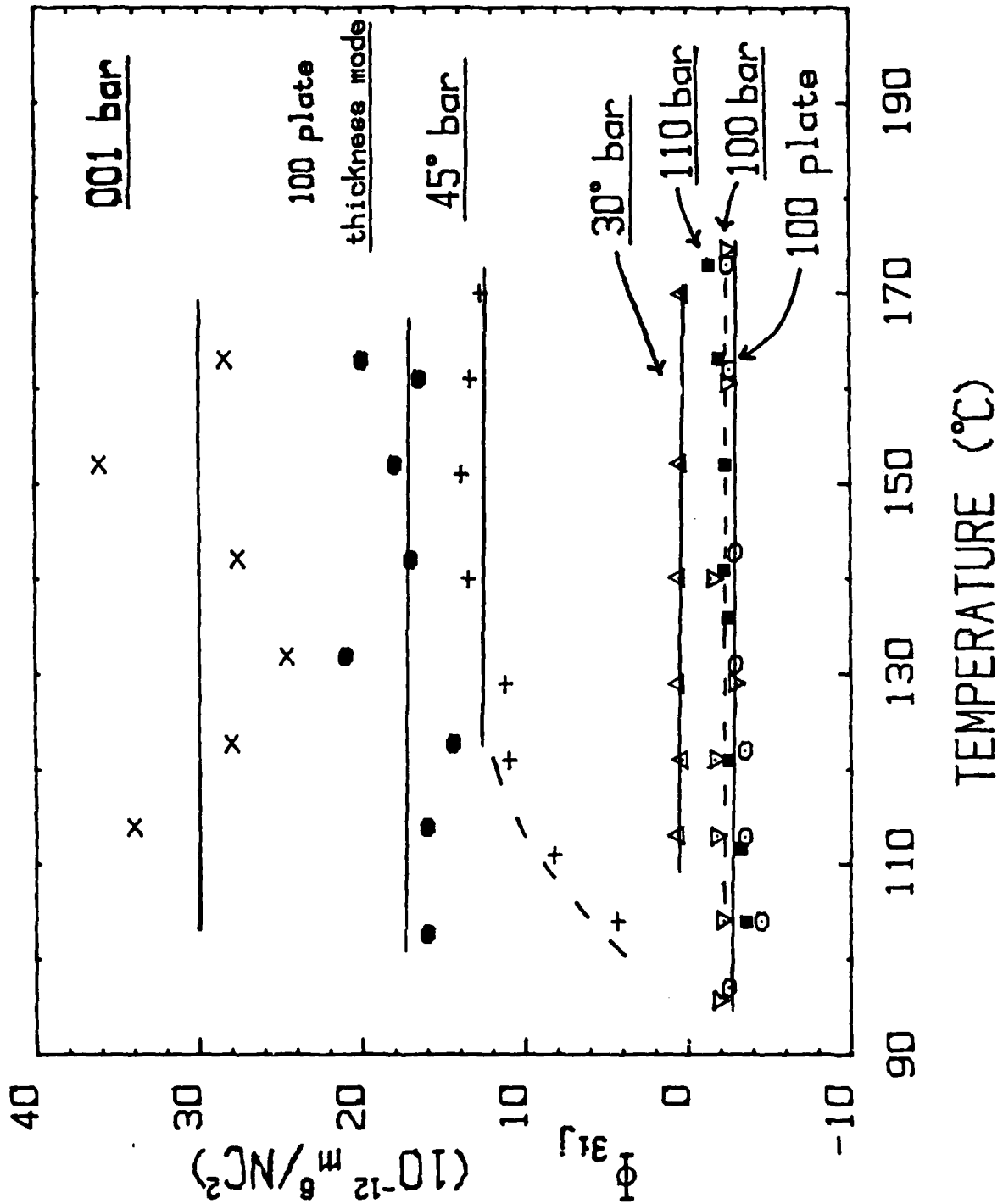


Fig. 3 Measured values of rotated and unrotated cuts over a range of temperature above T_c .



ERC41007.14SA

Table 1 Determined Thermodynamic Parameters

$\alpha_{10} =$	$3.72 \times 10^{-6}/^{\circ}\text{C}$	Q_{31}	$-0.71 \times 10^{-2} \text{ m}^4/\text{coul}^2$
α_{30}	$2.52 \times 10^{-6}/^{\circ}\text{C}$	Q_{33}	3.0 *(3.4)
θ_1	-379°C	Q_{44}	1.38
θ_3	76°C	ϕ_{311}	$-2.2 \times 10^{-12} \text{ m}^6/\text{N-coul}^2$
T_c	77°C	ϕ_{312}	-3
α_{13}	$4.2 \times 10^{-3} \text{ MKS}$	ϕ_{313}	-5
α_{133}	4.22×10^{-2}	ϕ_{333}	+28
α_{1333}	4.98×10^{-2}	ϕ_{334}	+35 **(16)
α_{33}	-1.74×10^{-2}	ϕ_{366}	-3
α_{333}	30.2		

*The electrostriction constant (Q_{33}) as determined from the strain P_s data.

**The higher order ϕ_{334} constant determined from the 30° bar. Believed to be the truer value, since less dependent on possible "anomalous" behavior found in the 001 polar direction.

change at T_c . It may be used, however, also in good approximation to describe a crystal with a diffuse transition if the transition temperature T_c is presumed to be distributed.

The choice of the distribution function and the stiffness parameters is rigorously limited by the need to fit the observed dielectric permittivity and spontaneous electric polarization data. For the 61:39 SBN the chosen parameters are



$$T_c - \theta = 1^\circ\text{C}$$

$$P_0 = 1.7 \times 10^{-2} \text{ C/m}^2$$

$$T_c = 77^\circ\text{C}$$

The distribution of Curie points is nearly Gaussian with a halfwidth $\Delta T \cong 8^\circ\text{C}$. For these parameters, measured and calculated polarization P_s is shown in Fig. 4.

Using the distributed P_s data and the experimental dielectric data, the dielectric stiffnesses were determined and reported in Table 1. Up to sixth order stiffnesses (α_{ijklmn}) were necessary to achieve a reasonable correlation between the experimental and phenomenological derived values, (see Fig. 5).

The electrostriction constants (Q_{ijkl}) reported in Table were derived from Eq. (16) and found to be comparable with those measured for other tetragonal bronzes.⁹ A Q_{33} value of $3.4 \times 10^{-2} \text{ m}^4/\text{C}^2$ similar to that derived using Eq. (16) was determined from the strain/ P_s data near room temperature. From the spontaneous elastic strain determined for the Q_{33} value of $0.034 \text{ m}^4/\text{C}^2$ (Eq. (15)), the ferroelectric contribution to the thermal expansion (α_3) along "c" was determined, shown in Fig. 6.

If the resonance and antiresonance measurements are carried on down into the ferroelectric phase below T_c , the same crystal cuts may be used to measure S_{ij}^P and S_{ij}^E in the single domain ferroelectric species. A crucial test of the predictive capability of the extended LGD method may then be made

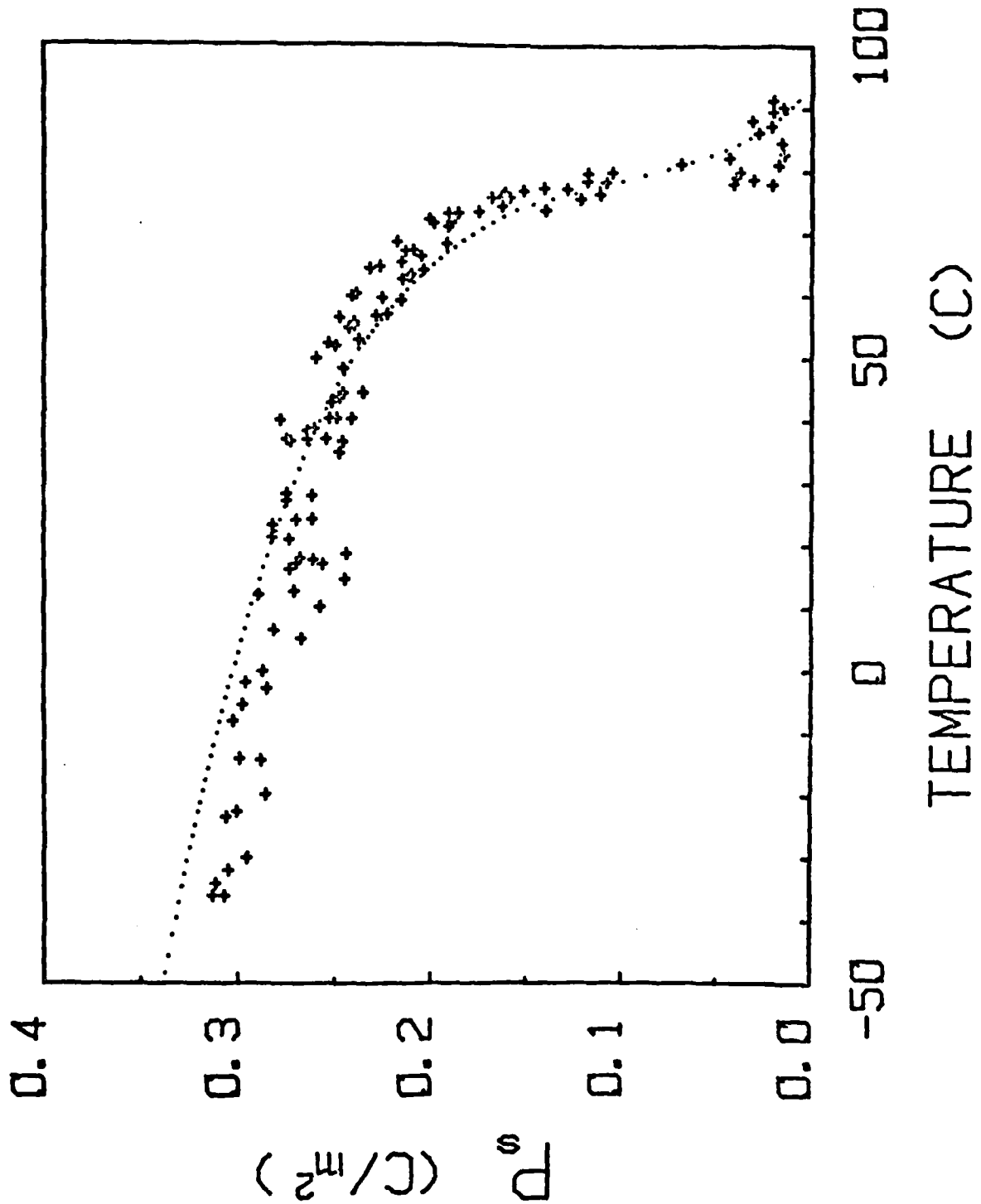


Fig. 4 Comparison of the measured P_s in SBN and distribution function values.



ERC41007.14SA

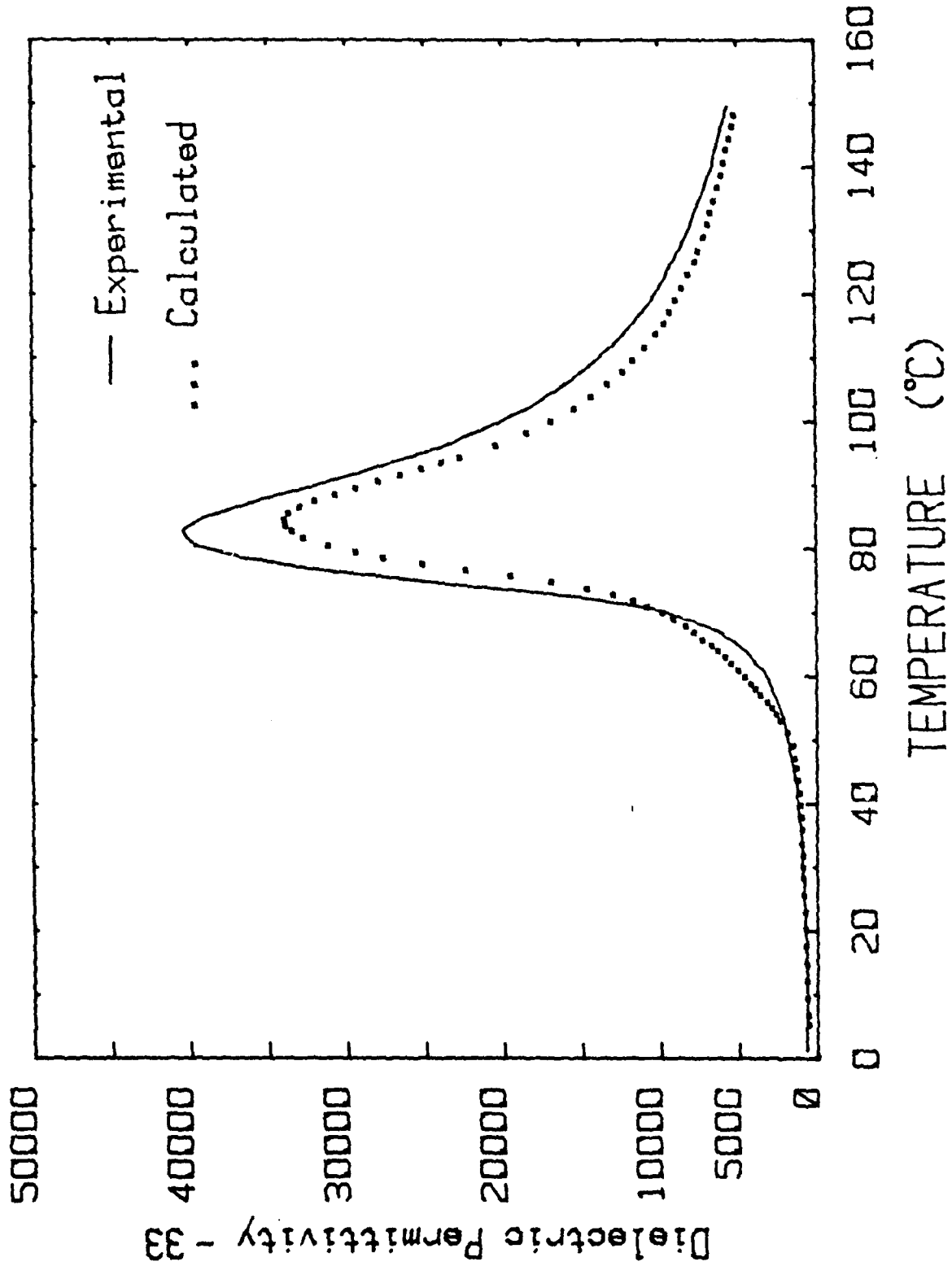


Fig. 5 Measured weak field permittivity ϵ_{33} for SBN compared to the calculated using the distributed LGB model.



ERC41007.14SA

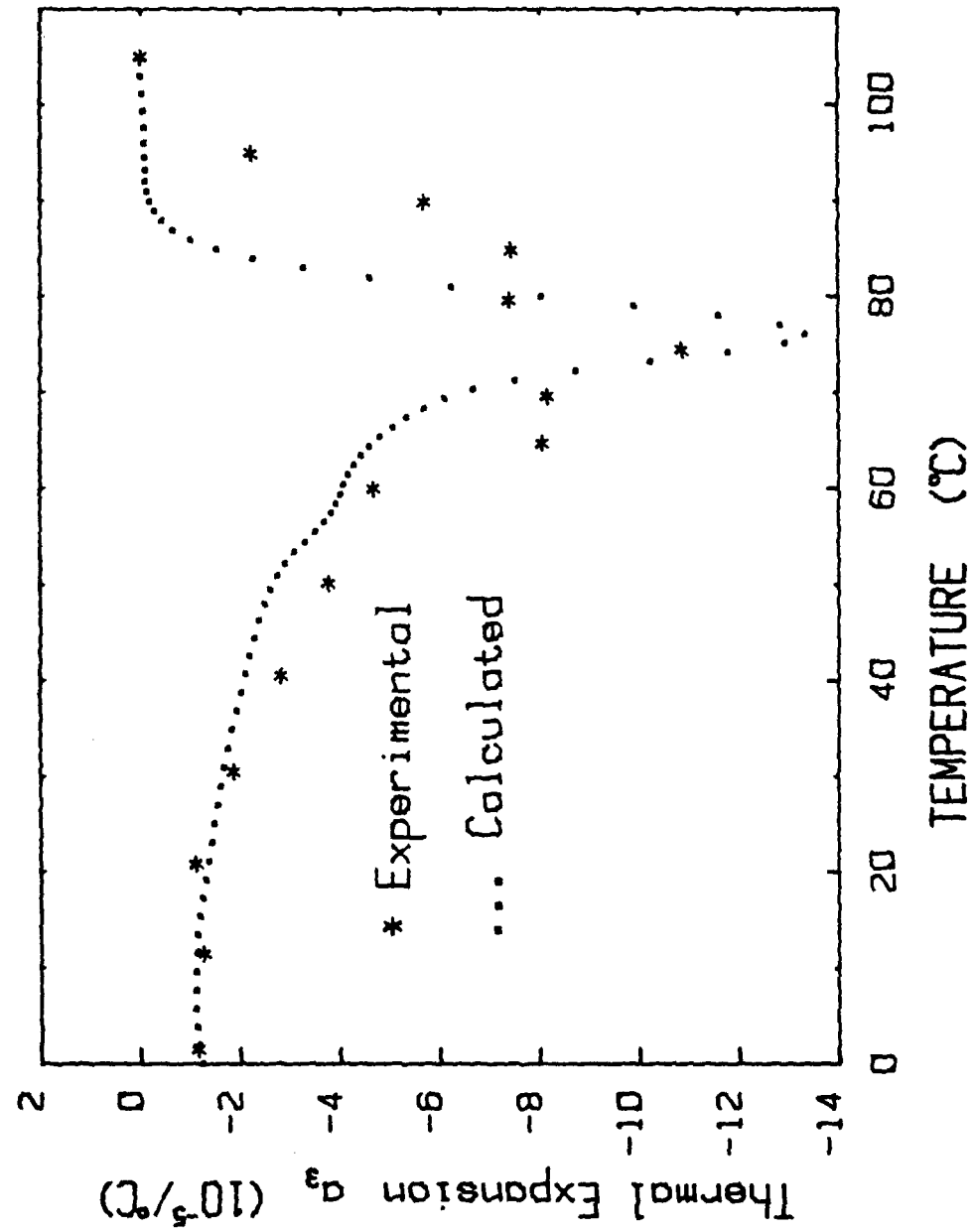


Fig. 6 Measured and desired thermal expansion a_3 .



ERC41007.14SA

by comparing calculated S_{ij} constants derived using the measured high temperature ϕ_{3ij} values and known P_s and the experimentally determined constants. Such comparisons for S_{11}^P , S_{12}^P and S_{44}^P are shown in Figs. 7.

The agreement for S_{44}^P is excellent. For S_{11}^P and S_{12}^P however there are clear compliance maxima near T_c which are not predicted. This breakdown of the simple theory is not however completely unexpected. Since the LGD phenomenology neglects all thermal fluctuations, and such fluctuations must become large close to a near 2nd order phase change, it is evident that p^2 will not be zero just above T_c and an elastic softening through the normal electrostrictive effect is to be expected.¹⁰

If this contribution due to fluctuations is assumed to be symmetrical about T_c then its effect can be removed and the agreement between theory and experiment for temperatures close to T_c is correspondingly improved.

Measurements of S_{33}^P show a very large compliance peak at T_c and the effect of fluctuations here is much too large to correct by the simple subtraction procedure.

The complete set of electro-acoustic constants for the 61:39 SBN composition are summarized in Table 2, and the room temperature coefficients are also given in Table 2. Except for the measured S_{33}^P , calculated and predicted constants are in good agreement.

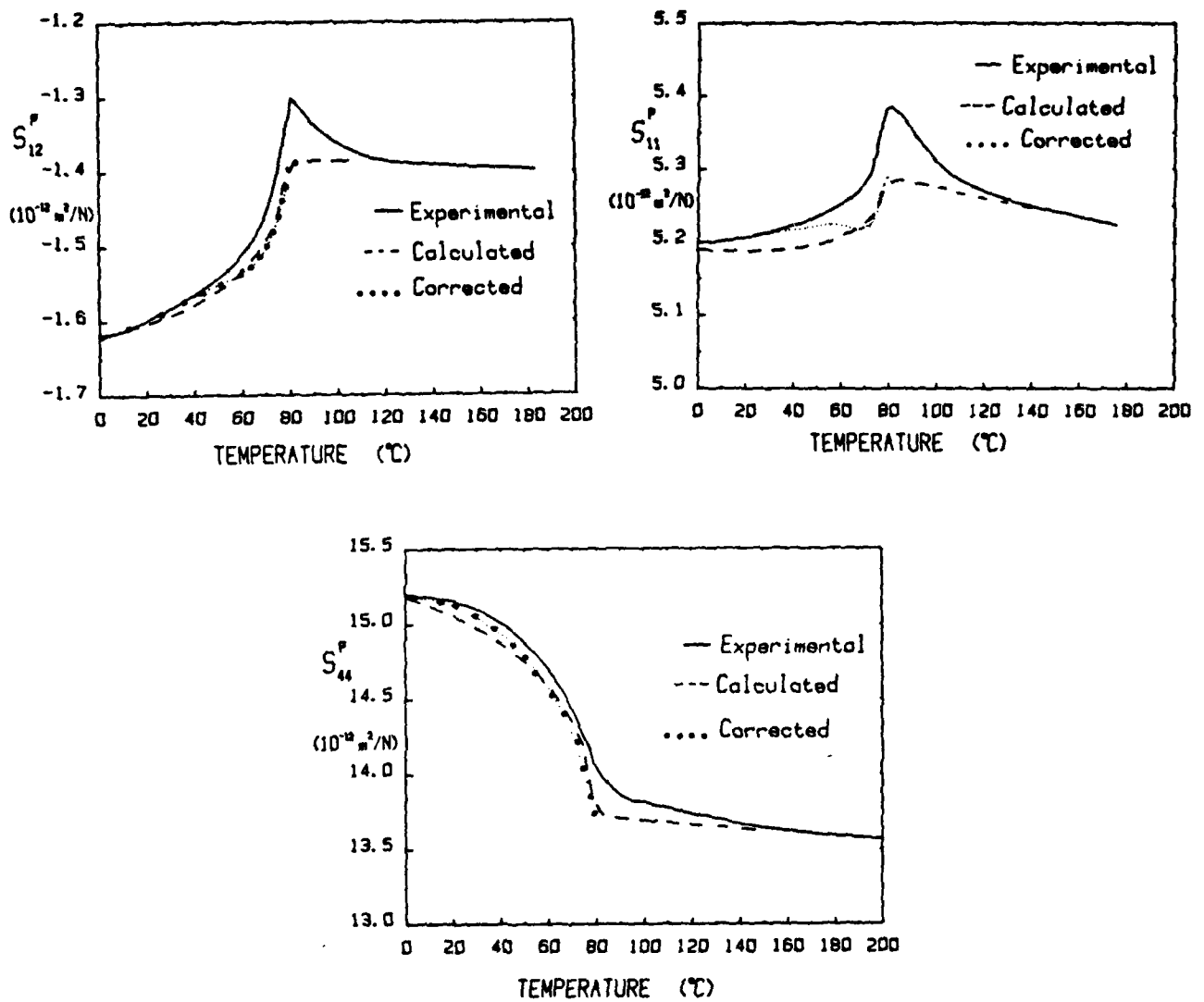


Fig. 7 S_{ij}^P measured from piezo-electric response data compared to S_{ij}^P derived using ϕ_{3ij} values determined in the paraelectric phase.



Table 2 Physical Constants of SBN at Room Temperature

$\epsilon_{11}^x/\epsilon_0$	470	$*\epsilon_{11}^x/\epsilon_0$	462	$T_{S_{11}}^P$	$-1.2 \times 10^{-4}/^\circ\text{C}$
$\epsilon_{33}^x/\epsilon_0$	880	$*\epsilon_{33}^x/\epsilon_0$	633	$T_{S_{12}}^P$	-9.2
S_{11}^E	$5.32 \times 10^{-12} \text{ m}^2/\text{N}$	S_{11}^P	$5.21 \times 10^{-12} \text{ m}^2/\text{N}$	$T_{S_{13}}^P$	-.63
S_{12}^E	-1.46	S_{12}^P	-1.56	$T_{S_{33}}^P$	-5.0
S_{13}^E	-1.73	S_{13}^P	-2.21	$T_{S_{44}}^P$	+2.3
S_{33}^E	10.10	S_{33}^P	7.82	$T_{S_{66}}^P$	-.80
S_{44}^E	15.48	S_{44}^P	15.22	$T_{\epsilon_{11}}^x$	$-4.8 \times 10^{-3}/^\circ\text{C}$
S_{66}^E	14.4	S_{66}^P	14.4	$T_{\epsilon_{31}}^x$	-.20
d_{15}	$31 \times 10^{-12} \text{ C/N}$	k_{15}	13	$T_{d_{15}}$	$-.08 \times 10^{-2}/^\circ\text{C}$
d_{31}	-30	k_{31}	14	$T_{d_{31}}$	-1.07
d_{33}	130	k_{33}	47.5	$T_{d_{33}}$	-1.23
$**_1$	$8 \times 10^{-6}/^\circ\text{C}$	$k_t(\text{thickness})$	44	$T_{k_{15}}$	$-.02 \times 10^{-3}/^\circ\text{C}$
$'_3$	-8	$k_p(\text{planar})$	21	$T_{k_{31}}$	-.99
	$5.29 \times 10^3 \text{ hg/m}^3$			$T_{k_{33}}$	-1.36

*Dielectric permittivities at constant strain (x) were measured using a model 419JA RF impedance analyzer at a frequency greater than 50 MHz.

**Note: The thermal expansion coefficient α not to be confused with the LGD α 's as in equation (6).



Taken together with the strong dimensional coupling through Q_{33} which leads to the "anomalous" negative thermal expansion $\alpha_{\lambda(3)}$ (Fig. 6), the positive ϕ_{344} and ϕ_{33} values do suggest that the bronze structure family will be of considerable interest as temperature compensated acoustic wave materials. Measurements which tend to confirm these characteristics for the SBN will be reported elsewhere.

There is as yet too little experimental information from other bronze family crystals to confirm the general utility of the phenomenological approach. However a promising note that both S_{44}^P and S_{33}^P do soften with decreasing temperature for the tetragonal bronze KTN as reported in reference 11. The fact that seven ferroelectric species are theoretically possible while only two are actually observed in the hundreds of bronze ferroelectrics so far studied suggests that the higher order dielectric stiffnesses (α^{ijkl} , α_{ijklmn}) have a very limited range of values. That the Q constants change little with cationic makeup is confirmed by available data⁹ on Q_{11} from spontaneous polarization and spontaneous strain measurements in the orthorhombic bronzes.

If the Q constants do not change significantly, it is then logical to expect that the higher order ϕ constants will also be insensitive to cationic makeup but there is urgent need for more experimental data to confirm this hypothesis.

2.5 Conclusions

(i) A complete set of electro-acoustical parameters are reported for $(\text{Sr}_{0.61}\text{Ba}_{0.39}\text{Nb}_2\text{O}_6)$; (ii) The LGD phenomenology for simple proper ferroelectrics has been extended to include sixth order coupling parameters; (iii) Sixth order ϕ_{ijklmn}



constants can be used to predict the elastic behavior for temperatures outside the Curie range in these diffuse phase transition crystals, but additional "anomalous" softening occurs in the mixed phase Curie region; (iv) The observed behavior is consistent with higher order constants being only weakly composition and temperature dependent, but additional measurements of the ϕ constants in other ferroelectric bronzes are urgently needed: (v) the phenomenological method does permit the correlation of low temperature data in the ferroelectric phase with a limited family of temperature independent higher order constants of the simpler paraelectric symmetry and with accumulating experience, the possibility of predicting dielectric, thermal, piezoelectric and elastic response and its temperature dependence for all simple proper bronze ferroelectrics.



3.0 MATERIALS PREPARATION AND CHARACTERIZATION

3.1 Single Crystal Growth of $\text{Sr}_{.61}\text{Ba}_{.39}\text{Nb}_2\text{O}_6$

The Czochralski single crystal growth technique has successfully been developed to the congruent melting composition $\text{Sr}_{.61}\text{Ba}_{.39}\text{Nb}_2\text{O}_6$. Detailed information on the compositional boundary conditions and phase diagram has already been discussed in our earlier reports. Although this process is now well established, the growth of multicomponent bronze systems is, in general, difficult, and success depends strongly on the ability to control the diameter of crystal and the thermal gradient in the crystal near the solid-liquid interface. During the past six months, considerable effort has been made to increase the diameter of SBN single crystals, and it was found possible to grow single crystals of one inch in diameter. Beyond this limit, however, growth was found to be difficult and crystal tended to crack because of stiff thermal gradients in the crystals. Optimum growth conditions used for one inch diameter crystals are as follows:

Pulling Rate:	8-10 mm/hr
Growth Direction	Along the C-axis
Growth Temperature	1500-1510°C
Atmosphere	Oxygen for platinum crucible

Fracture free and optically good quality single crystals, approximately one inch in diameter and two inches long have been produced. Crystals are pale yellow color, but become deep yellow when the crystal diameter is greater than 1.5 cm.



Crystals grown along the c-axis are usually well faceted, which is exceptional for Czochralski grown crystals. As shown in Fig. 8, the SBN single crystal showed 24 faces of four prisms: (110), (120), (100), and (130). Faces of the (100) and (110) forms are best developed on crystals with high strontium content. Using these two forms, the SBN single crystals could be oriented with minimum problems.

3.2 Characterization of Bulk Single Crystals

Optically, the $\text{Sr}_{.61}\text{Ba}_{.39}\text{Nb}_2\text{O}_6$ single crystals appear to be good quality crystals that are clear and transparent. Crystals showed room temperature tungsten bronze tetragonal structure and, according to the structural refinements by Jamieson et al (12) for $\text{Sr}_{.75}\text{Ba}_{.25}\text{Nb}_2\text{O}_6$ crystals, this solid solution belongs to the point group 4 mm. The lattice parameter measurements for the ceramic and single crystals samples of the $\text{Sr}_{.61}\text{Ba}_{.39}\text{Nb}_2\text{O}_6$ composition gave values of $a = 12.452 \text{ \AA}$ and $c = 3.938 \text{ \AA}$, which are in close agreement with the values $a = 12.461 \text{ \AA}$ and $c = 3.936 \text{ \AA}$ reported by Megumi et al (13) for the same composition.

3.2.1 Poling Procedure

To obtain optimum data concerning surface acoustic wave velocity and electro-optic or even nonlinear properties of ferroelectric crystals, it is necessary to work with single domain pieces. Therefore, it is important in the present work to prepare single domain SBN single-crystal for evaluation of their acoustical properties. Based on our temperature dependence dielectric measurements (given in Fig. 9) on the $\text{Sr}_{.61}\text{Ba}_{.39}\text{Nb}_2\text{O}_6$ single crystals, the ferroelectric transition temperature (T_c) occurs around 72°C ; this information is absolutely

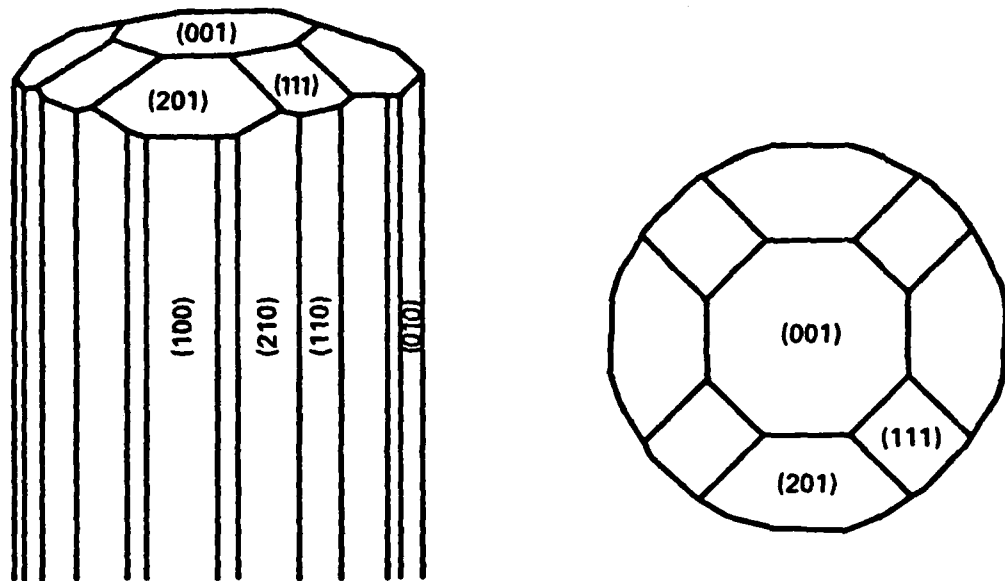


Fig. 8 Idealized form of the SBN single crystals.

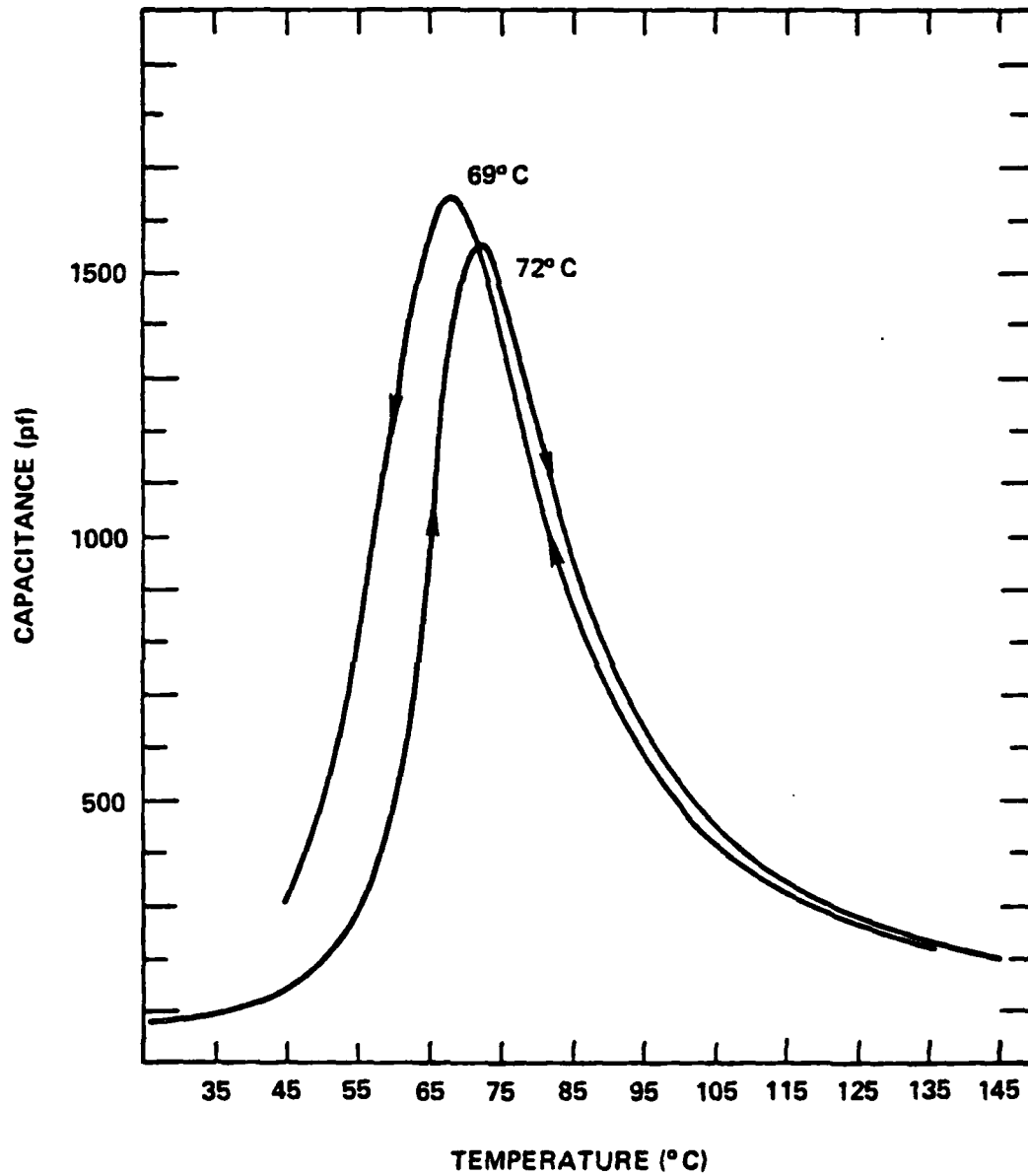


Fig. 9 Capacitance as a function of temperature for the SBN single crystal.



CRC41007.14SA

required. The procedure for poling used here consisted of heating the grown SBN single crystal to about 5°C below T_c , with dc field between 1 to 6 KV/cm along the c-axis of the sample, for a time corresponding to one hour per cm length. The electrode material used is either gold or aluminum, and care must be taken to be sure that the leads to sample do not contact the furnace walls. The latter are more conducting than the sample at elevated temperatures. As shown in Fig. 10, an approximately 5.0 V/cm field was needed to obtain single domain $\text{Sr}_{.61}\text{Ba}_{.39}\text{Nb}_2\text{O}_6$ single crystal.

SBN wafers with crystallographic orientations (100) and (110) have also been poled successfully. The well established technique for the SBN single crystals will make it possible to evaluate their acoustical as well as piezoelectric properties.

3.2.2 Method for Evaluating SAW Electromechanical Coupling Constants

The excitation of surface acoustic waves depends on the electro-mechanical coupling coefficient k , which is a function of the piezoelectric medium and geometry of the transducer configuration. A number of methods to establish this coupling exists; however, the present study uses the equivalent circuit technique given by Smith et al (14), which only requires a Boonton RX meter. The relationship between the coupling constant and the equivalent parallel resistance and capacitance is

$$k^2 = \frac{1}{8 N C_p R_p f_o} \cdot$$



ERC41007.14SA

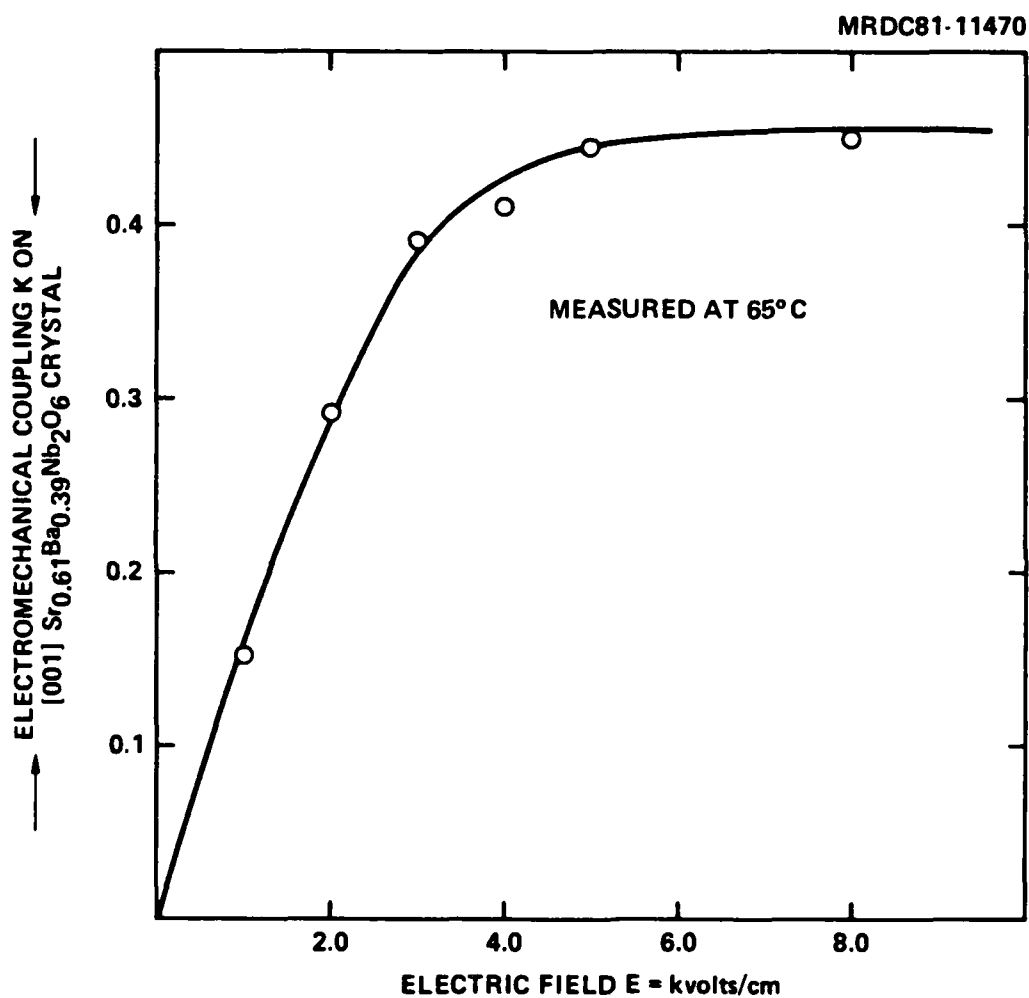


Fig. 10 Electromechanical coupling constant as a function of applied field.



The SAW electromechanical coupling constant, k^2 , for three different cuts, e.g., (100), (110) and (001) of $\text{Sr}_{.61}\text{Ba}_{.39}\text{Nb}_2\text{O}_6$ bulk single crystal has been determined and is given in Table 3. The coupling constant has been shown to be large for the (001) plane propagation along the $\langle 110 \rangle$ direction, and its value is measured to be 422×10^{-4} which is comparable to the Y-Z cut LiNbO_3 crystals (480×10^{-4}). Untuned insertion losses for the SBN crystals were found to be substantially lower than LiNbO_3 crystals due to the higher dielectric constant of SBN which produced a much lower impedance transducer. This makes the material very attractive for applications where the transducer beamwidth must be small (i.e. concludes). The temperature coefficient of time delay for the Z-cut surface wave delay lines was measured and is shown in Fig. 11. The results make it clear that this material possesses a temperature compensated orientation.

Table 3 Electromechanical Coupling Constant k^2 for SBN Crystal

PLANE/DIRECTION	PHASE VELOCITY	SAW k^2 ($2 \frac{v}{V}$)
(001)/ $\langle 100 \rangle$	3675 M/Second	422×10^{-4}
(100)/ $\langle 001 \rangle$	3545 M/Second	147×10^{-4}
(110)/ $\langle 001 \rangle$	3528 M/Second	147×10^{-4}

3.3 Liquid Phase Epitaxial Growth of $\text{Sr}_{1-x}\text{Ba}_x\text{Nb}_2\text{O}_6$

As we discussed in the earlier reports, the LPE growth technique has successfully been developed for the ferroelectric $\text{Sr}_{.5}\text{Ba}_{.5}\text{Nb}_2\text{O}_6$ composition by using

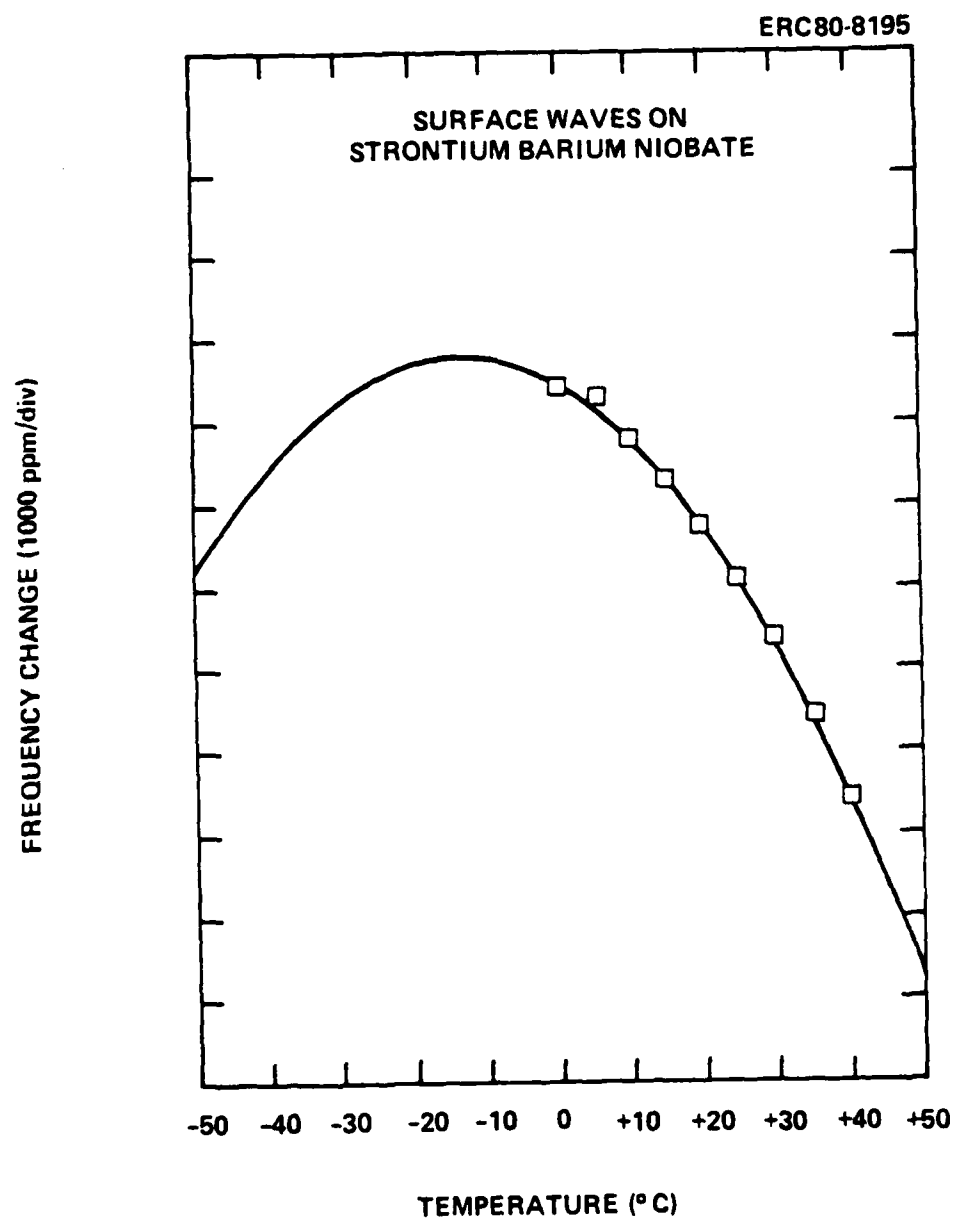


Fig. 11 The temperature coefficient of time delay for the z-cut SBN surface wave delay lines.



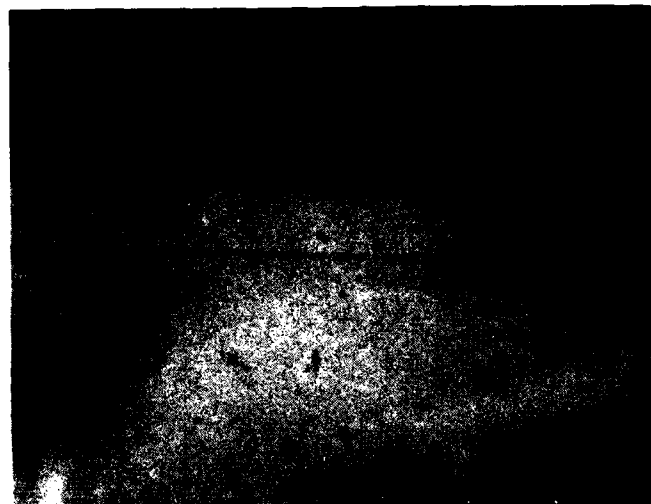
the BaV_2O_6 solvent. The liquids temperature and compositional boundary conditions for this composition were determined by establishing the phase diagram for the binary system $\text{BaV}_2\text{O}_6\text{-Sr}_{.5}\text{Ba}_{.5}\text{Nb}_2\text{O}_6$. Based on this work, the mixture containing 70 mole% BaV_2O_6 and 30 mole% $\text{Sr}_{.5}\text{Ba}_{.5}\text{Nb}_2\text{O}_6$ was found to be suitable because (1) the composition of resulting phase is close to $\text{Sr}_{.5}\text{Ba}_{.5}\text{Nb}_2\text{O}_6$, and (2) the composition melts at relatively lower temperature (950°C). Detailed information on this system is provided in our earlier report.

Initially the Z-cut $\text{Sr}_{.61}\text{Ba}_{.39}\text{Nb}_2\text{O}_6$ substrates were used, and the process was established for this composition. Films as thick as $20\text{-}25\text{ }\mu\text{m}$ were easily grown at about 950°C . Figure 12 shows a typical cross section of $\text{Sr}_{.5}\text{Ba}_{.5}\text{Nb}_2\text{O}_6$ film on the SBN substrate. Films grown from the vanadium containing solvent are dark amber to yellow in color, and the surface of the films is smooth and clear. Based on the lattice constant determination by the x-ray diffraction technique for the reflections (001) and (002), the films indicate that the composition is close to $\text{Sr}_{.5}\text{Ba}_{.5}\text{Nb}_2\text{O}_6$. Recently, the efforts have been extended to study the directional dependence growth of this composition. Other crystallographically preferred orientations such as (100), (110) and (111) have been selected for this task, and work is already in progress. A few LPE runs on the (100) cut indicate that the growth is possible on this surface, but further work to establish the experimental parameters as well as composition of the films is required. Since SBN crystallizes at much faster rate along the c-axis, the LPE growth on the other direction is expected to be much slower and more difficult.



ERC41007.14SA

SC78-3045



— FILM (20μm)

← SUBSTRATE

Fig. 12 Shows a typical cross section of the $\text{Sr}_{.5}\text{Ba}_{.5}\text{Nb}_2\text{O}_6$ film on the Z-cut SBN substrate.



Once this work is completed for the composition $\text{Sr}_{.5}\text{Ba}_{.5}\text{Nb}_2\text{O}_6$, the efforts will be extended to another composition, $\text{Sr}_{.75}\text{Ba}_{.25}\text{Nb}_2\text{O}_6$. According to Lenzo et al (15), this composition exhibits highest electro-optic and piezoelectric properties and as such it is important to evaluate its acoustic properties. Since this composition is located at the Sr^{2+} -rich end of the BaV_2O_6 - SrNb_2O_6 - BaNb_2O_6 ternary system (Fig. 13), the compositions along BaV_2O_6 - SrNb_2O_6 binary join need to be examined in greater detail. Once this step is established, it will be possible to select proper composition for the LPE growth of $\text{Sr}_{.75}\text{Ba}_{.25}\text{Nb}_2\text{O}_6$ on the SBN substrates. It is also planned to initiate acoustical evaluation of such films, e.g. the SAW electromechanical coupling K^2 and the temperature stability using SAW resonators. Although the thin film growth of $\text{K}_3\text{Li}_2\text{Nb}_5\text{O}_{15}$ onto $\text{K}_2\text{BiNb}_5\text{O}_{15}$ by the rf sputtering technique, is known and reported by Adachi et al (16), this is the first time that the bronze compositions have been developed by the LPE technique. This opens a new interest in this family and it may be possible to obtain more complex and useful bronze compositions by using this novel technique.

3.4 Crystal Chemistry of PbNb_2O_6

The work on the $\text{Pb}_{1-2x}\text{K}_x\text{La}_x\text{Nb}_2\text{O}_6$ solid solution was continued to establish temperature dependence dielectric properties. According to our x-ray powder diffraction work, three structurally different phases, orthorhombic tungsten bronze, tetragonal tungsten bronze, and paraelectric $\text{K}_{.5}\text{La}_{.5}\text{Nb}_2\text{O}_6$ type tetragonal phase have been identified for this solid solution. Among these three phases, the orthorhombic phase extends over a wide compositional range between $0.0 < x < 0.50$. The experimental results have briefly been presented in Table 4.



ERC41007.14SA

ERC79-7149

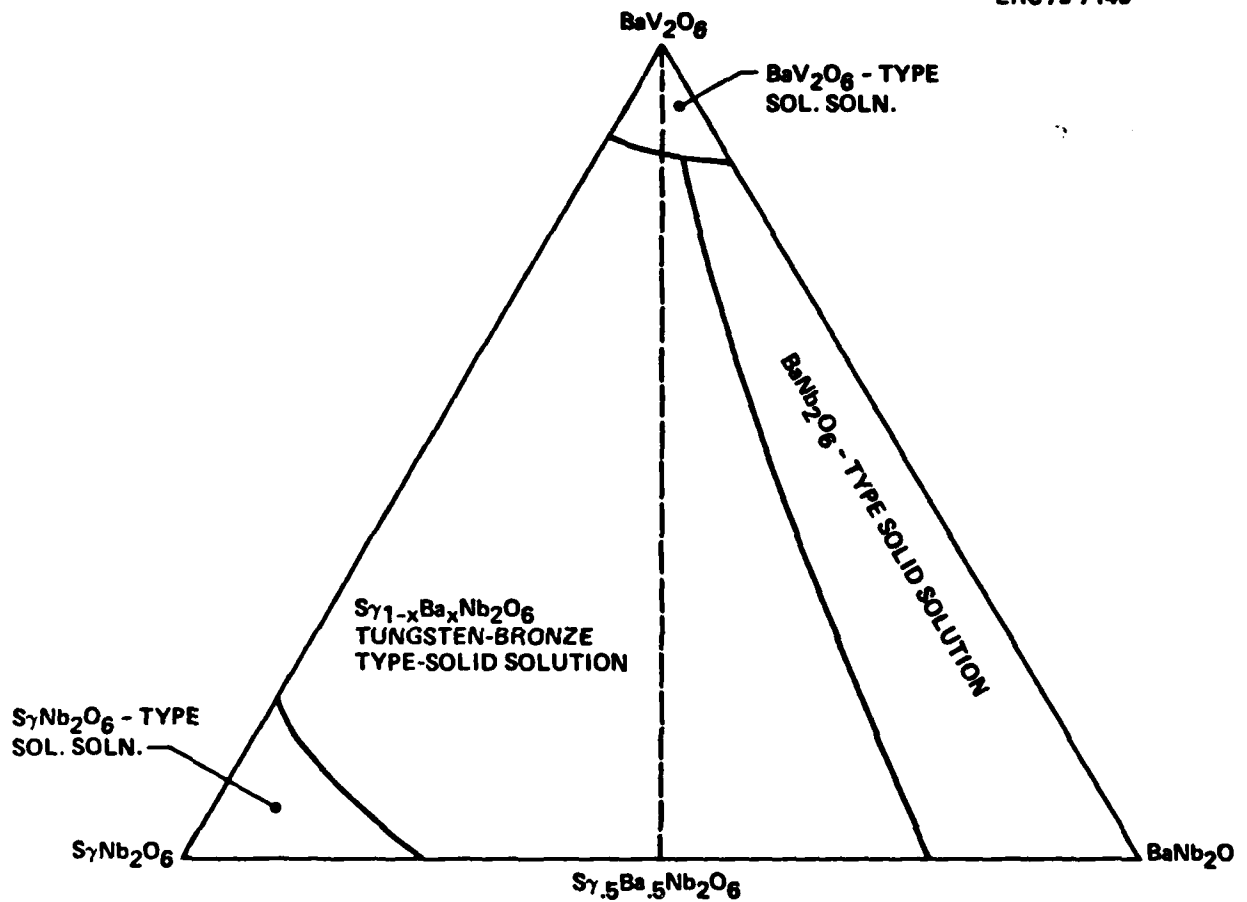


Fig. 13 The system BaV_2O_6 - SrNb_2O_6 - BaNb_2O_6 , in air at 1200°C .

Table 4 The Solid - Solution Based on the PbNb_2O_6 system

Composition	Symmetry	Unit A_A°	Cell b_A°	Diminsions C_A°	Ferroelectric T_C°
PbNb_2O_6	Orthorhombic	17.630	17.930	3.868	570
$\text{Pb}_{.90}\text{K}_{.05}\text{La}_{.05}\text{Nb}_2\text{O}_6$	"	17.653	17.883	3.880	450
$\text{Pb}_{.80}\text{K}_{.10}\text{La}_{.10}\text{Nb}_2\text{O}_6$	"	17.677	17.836	3.896	350
$\text{Pb}_{.70}\text{K}_{.15}\text{La}_{.15}\text{Nb}_2\text{O}_6$	"	17.685	17.807	3.900	202
$\text{Pb}_{.60}\text{K}_{.20}\text{La}_{.20}\text{Nb}_2\text{O}_6$	"	17.706	17.777	3.904	100
$\text{Pb}_{.50}\text{K}_{.25}\text{La}_{.25}\text{Nb}_2\text{O}_6$	"	12.520	-	3.914	-3*
$\text{Pb}_{.40}\text{K}_{.30}\text{La}_{.30}\text{Nb}_2\text{O}_6$	"				-100*
$\text{Pb}_{.20}\text{K}_{.40}\text{La}_{.40}\text{Nb}_2\text{O}_6$	"				
$\text{K}_{.5}\text{La}_{.5}\text{Nb}_2\text{O}_6$	"	17.68	-	7.80	-

The Curie temperature, T_C , is known to be one of the fundamental characteristics of ferro- and antiferroelectrics. This measurement gives the origin of the spontaneously polarized state and is considered important for characterizing the piezoelectric materials. In our present work, the T_C for the $\text{Pb}_{1-2x}\text{K}_x\text{La}_x\text{Nb}_2\text{O}_6$ solid solution system has been obtained by measuring the dielectric properties as a function of temperature. The technique is relatively simple and the measurements have been performed routinely, using a capacitance bridge (HP 4270A). The test specimen (Disks) used for the dielectric measurements are approximately 1.3 cm in diameter and 0.3 cm thick and are coated on each side with platinum by the standard vacuum evaporation technique.



ERC41007.14SA

PbNb_2O_6 is very useful ferroelectric material and exhibits the ferroelectric transition temperature, T_c , around 570°C (17-18). The addition of $\text{K}^+ + \text{La}^{3+}$ for 2 Pb^{2+} in the PbNb_2O_6 shifted the T_c towards a lower temperature in both the orthorhombic and the tetragonal tungsten bronze solid solutions. Figure 14 shows a variation of ferroelectric transition temperature as a function of $\text{K}^+ + \text{La}^{3+}$ concentration. The system $\text{Pb}_{1-x}\text{Ba}_x\text{Nb}_2\text{O}_6$ has also been studied by several workers (19-22) and, according to their findings, the ferroelectric transition temperature first decreases in the orthorhombic tungsten bronze phase and then increases on further addition of Ba^{2+} in the tetragonal tungsten bronze phase. Although both these system are structurally similar, their ferroelectric properties appear to be significantly different. Further work is in progress on the $\text{Pb}_{1-2x}\text{K}_x\text{La}_x\text{Nb}_2\text{O}_6$ system to understand its ferroelectric behavior.

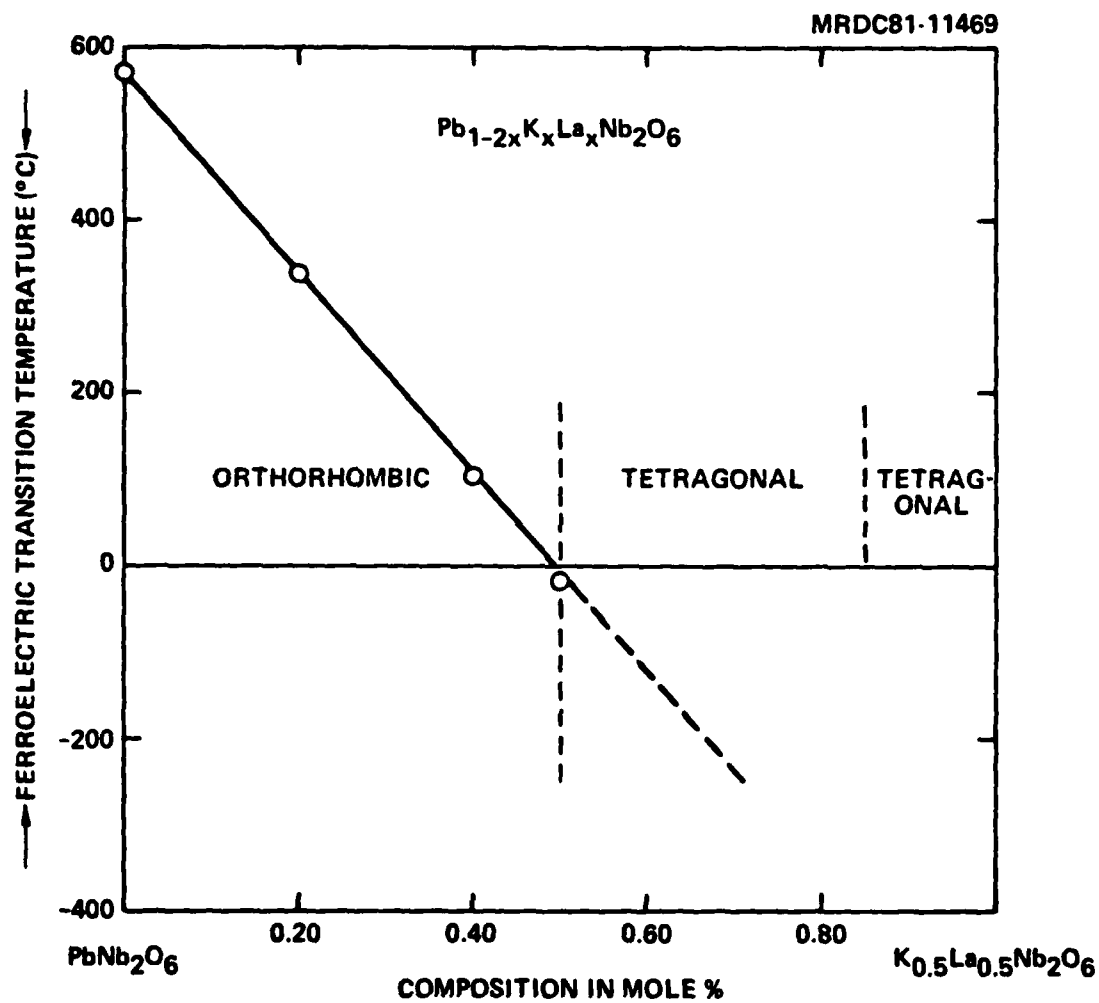


Fig. 14 Variation of ferroelectric transition temperature for the $Pb_{1-2x}K_xLa_xNb_2O_6$ system.



4.0 FUTURE PLANS

4.1 Application of Phenomenological Model

Based on the phenomenological analysis on the tungsten bronze family, it has been shown that the six order electrostriction constants ϕ_{ijklmn} play a most important role in studying the elastic behavior in the single domain ferroelectric phase. This work will be continued to obtain more information on the bronze family.

4.2 Materials Preparation and Acoustic Characterization

The liquid phase epitaxial (LPE) technique has been shown to be successful to develop the $\text{Sr}_{.5}\text{Ba}_{.5}\text{Nb}_2\text{O}_6$ films onto the SBN substrate using the BaV_2O_6 flux. During the next six months, efforts will be made to determine compositional boundary conditions for the other important composition $\text{Sr}_{.75}\text{Ba}_{.25}\text{Nb}_2\text{O}_6$ since this composition exhibits highest electro-optic and pyroelectric coefficients. We also plan to initiate LPE growth $\text{Sr}_{.5}\text{Ba}_{.5}\text{Nb}_2\text{O}_6$ composition on other cuts such as (100), (110) and (111).

Bulk single crystal characterization to determine optimum values of the surface acoustic wave electromechanical coupling (K^2) and the temperature dependence coefficient work will be continued on the orientations, e.g. (100), (110) and (111) etc., of $\text{Sr}_{.61}\text{Ba}_{.39}\text{Nb}_2\text{O}_6$ single crystals. Measurements will also be made to determine the elastic, dielectric and piezoelectric constants as a function of temperature for different cuts and orientations.



4.3 Electro-Optic Measurements

Electro-optic measurements will be made to determine r_{13} and r_{33} coefficients of $\text{Sr}_{.61}\text{Ba}_{.39}\text{Nb}_2\text{O}_6$ single crystals. Once this is established, the crystals will be tested for the electro-optic Fabry-Perot spectral filter application.

4.4 Crystal Chemistry

The temperature dependence dielectric measurements on the $\text{Pb}_{1-2x}\text{Na}_x\text{La}_x\text{Nb}_2\text{O}_6$ system will be initiated to evaluate its ferroelectric properties.



5.0 PUBLICATIONS AND PRESENTATIONS

5.1 Publications

1. R. R. Neurgaonkar, T. C. Lim, E. J. Staples and L. E. Cross, "An Exploration of the Limits of Stability of the LiNbO_3 Structure Field with A and B Site Cation Substitutions, Ferroelectrics," Vol. 27-28 (1980) 63-66.
2. K. L. Keester, R. R. Neurgaonkar, T. C. Lim and E. J. Staples, "Strontium Metaniobates: Its Crystallography, Polimorphism and Isomorphism," Mat. Res. Bull.
3. R. R. Neurgaonkar, M. H. Kalisher, T. C. Lim, E. J. Staples and K. L. Keester, "Czochralski Single Crystal Growth of $\text{Sr}_{.61}\text{Ba}_{.39}\text{Nb}_2\text{O}_6$ for Surface Acoustic Wave Devices," Submitted to Mat. Res. Bull. 15, 1235, 1980.
4. L. E. Cross, R. Betch, H. Mckinstry, T. Shrout and R. R. Neurgaonkar, "A New Method for Predicting the Temperature Dependence of Elastic Compliance in Simple Proper Ferroelectrics," Proceedings of Frequency Control Symposium, 1980.
5. R. R. Neurgaonkar and W. K. Cory, "Structural and Dielectric Properties of $\text{Ba}_6\text{Ti}_2\text{Nb}_8\text{O}_{30}$ Type Tungsten Bronze Compositions," (In preparation).
6. R. R. Neurgaonkar, T. C. Lim, E. J. Staples and L. E. Cross, "Crystal Chemistry of Ferroelectric Materials for SAW Devices," Proceedings of Ultrasonic, 1980.



7. T. R. Shrout, L. E. Cross, P. Moses, H. A. McKinstry and R. R. Neurgaonkar, "A Phenomenological Theory for Predicting the Temperature Dependence of Elastic, Dielectric and Piezoelectric Properties in Simple Proper Ferroelectric Crystals," Proceedings of Ultrasonic, 1980.

5.2 Presentations

1. R. R. Neurgaonkar, T. C. Lim, E. J. Staples and L. E. Cross, "An Exploration of the Limits of Stability of the LiNbO_3 Structural Field with A and B Site Cation Substitutions," Presented at the IEEE Int. Sympo. of Ferroelectrics, Minneapolis, Minn. June 13-15, 1979.
2. K. L. Keester, R. R. Neurgaonkar, T. C. Lim and E. J. Staples, "Conoscopic Characterization of Czochralski Grown Strontium-barium Niobate Boules," Presented at the 4th Conf. on Crystal Growth, Stanford Sierra Camp, Fallen Leaf, California, May 16-18, 1979.
3. L. E. Cross, R. Betch, H. McKinstry, T. Shrout and R. R. Neurgaonkar, "A New Method for Predicting the Temperature Dependence of Elastic Compliance in Simple Proper Ferroelectric," Presented at the 34th Annual Symposium on Frequency Control, at Philadelphia, PA, May 28-30, 1980.
4. R. R. Neurgaonkar, T. C. Lim, E. J. Staples and L. E. Cross, "Crystal Chemistry of Ferroelectric Materials for SAW Devices." Presented at the Annual Ultrasonic Symposium, Boston, Nov. 1980.



5. T. R. Shrout, L. E. Cross, P. Moses, H. A. McKinstry and R. R. Neurgaonkar,
"A Phenomenological Theory for Predicting the Temperature Dependence of
Elastic, Dielectric and Piezoelectric Properties in Simple Proper Ferro-
electric Crystals." Presented at the Annual Ultrasonic Symposium, Boston,
Nov. 1980.



6.0 REFERENCES

1. G. R. Barsch and R. E. Newnham, Piezoelectric Materials with Positive Elastic Constant Temperature Coefficients. AFCRL-TR-0163 Final Rpt. No. 19628-73-C-0108 (1975).
2. Landolt Bornstein, Ferro and Antiferroelectric Crystals, New Series, Vol. 3 & Vol. 9 (1969, 1973).
3. L. E. Cross, R. Betsch, H. McKinstry, T. Shrout and R. Neurgaonkar, Proc. 34th Ann. Freq. Control Symp., May 1980.
4. Jona and Shirane, Ferroelectric Crystals (1962).
5. J. F. Nye, Physical Properties of Crystals, Clarendon Press, Oxford, 1969.
6. D. Berlincourt and H. Jaffe, Phys. Rev. 111, 143 (1958).
7. B. Jaffe, W. R. Cook, Jr. and H. Jaffe, Piezoelectric Ceramics, Academic Press, London and New York, 1971.
8. For example: A.M. Glass, J. Appl. Phys. 40, 4699 (1969).
9. S. J. Jang, Electrostrictive Ceramics for Transducer Applications, Ph.D Thesis, The Pennsylvania State University, 1979.
10. M. Marutake, J. Phys. Soc. Jpn. 28, 214 (1970).
11. Adachi and A. Kawabata, Jpn. J. Appl. Phys. 11, 1969 (1978).
12. P. B. Jamieson, S. C. Abrahams and J. L. Bernstein, J. Chem. Phys. 48 (1968), 5048.
13. K. Megumi, N. Nagatsuma, Y. Kashiwada and Y. Furnhata, J. Mat. Sci. 11, 1976, 1583
14. Smith.



15. P. L. Lenzo, E. G. Spence and A. A. Ballman, Appl. Phys. Lett. 11, 1967, 23.
16. M. Adachi, T. Shiosaki and K. Kawabata, Ferroelectrics, 27 (1980), 89.
17. E. C. Subbarao, G. Shirane and F. Jona, Acta. Cryst. 13, 1960, 226
18. P. Labbe, M. Frey and A. Allais, Acta. Cryst. B. 29, 1973, 2204.
19. M. H. Francombe, Acta. Cryst. 13, 1960, 131.
20. V. A. Isupov and V. I. Kosiakov, Sov. Phys. - Tech. Phys. 3, 1958, 2002.
21. P. Baxter and H. N. J. Hellicar, J. Am. Ceram. Soc. 43, 1960, 578.
22. C. S. Brown, R. C. Kell, R. Taylor and L. A. Thomas, Proc. Inst. Elec. Engrs. (London), 109B, 1962, 99.